Internal Displacement Reactions in Multicomponent Oxides: Part I. Line Compounds with Narrow Homogeneity Range

S.N.S. REDDY, D.N. LEONARD, L.B. WIGGINS, and K.T. JACOB

As a model of an internal displacement reaction involving a ternary oxide "line" compound, the following reaction was studied at 1273 K as a function of time, t:

$$Fe + NiTiO_3 = \text{“Ni”} + \text{“}FeTiO_3\text{”}$$

Both polycrystalline and single-crystal materials were used as the starting $NiTiO_3$ oxide. During the reaction, the Ni in the oxide compound is displaced by Fe and it precipitates as a γ-(Ni-Fe) alloy. The reaction preserves the starting ilmenite structure. The product oxide has a constant Ti concentration across the reaction zone, with variation in the concentration of Fe and Ni, consistent with ilmenite composition. In the case of single-crystal $NiTiO_3$ as the starting oxide, the γ alloy has a "layered" structure and the layer separation is suggestive of Liesegang-type precipitation. In the case of polycrystalline $NiTiO_3$ as the starting oxide, the alloy precipitates mainly along grain boundaries, with some particles inside the grains. A concentration gradient exists in the alloy across the reaction zone and the composition is >95 at. pct Ni at the reaction front. The parabolic rate constant for the reaction is $k_p = 1.3 \times 10^{-12}$ m^2 s^{-1} and is nearly the same for both single-crystal and polycrystalline oxides.

I. INTRODUCTION

A displacement reaction between a metal and an oxide involves the reduction of a noble oxide by a reactive metal. Previous studies of solid-state displacement reactions between metals and oxides[1–6] have identified several types of reaction morphologies and their relationship to the thermodynamic and diffusional transport properties of product phases. Some of the reaction couples considered were Cu_2O/Co,[1] Cu_2O/Ni,[1] Cu_2O/Fe,[1,2] $Cu_2O/Co_{1-x}Fe_x$,[3] NiO/Fe,[1,4] NiO/Al,[5] and NiO/Mg.[6] In particular, Rapp *et al.*[1] have considered the reactive interface stability as a function of the diffusional rate control in the product phases. Internal reactions occur inside a metal or ceramic matrix; an example is the well-known internal oxidation of alloys.[7] Schmalzried[8,9] has considered internal oxidation and reduction reactions in multicomponent oxides and an extensive review is given by Schmalzried and Backhaus-Ricoult.[10] Shook *et al.*[11] have considered the internal displacement reaction in a metal matrix by studying the reaction between Cr and MoO_2 inside a Ni matrix. As part of a study of the internal displacement reactions in multicomponent oxides, the reaction between a metal and ternary oxide compound of a narrow homogeneity range (a line compound) is considered in this article, along with the results for a model reaction between Fe and $NiTiO_3$ at 1273 K. Reactions involving solid solutions of oxide compounds will be considered in Part II of this series of articles.[12] These reactions can be exploited to manufacture metal-ceramic composites having unique physical and mechanical properties.

II. DISPLACEMENT REACTIONS INSIDE A LINE COMPOUND

An internal displacement reaction in an oxide compound of a narrow homogeneity range is defined by the following chemical reaction:

$$\mathbf{A}\ (\text{metal}) + \mathbf{BCO}_{m+n}(\text{oxide}) = \text{“}\mathbf{B}\text{”}(\text{metal}) + \text{“}\mathbf{ACO}_{m+n}\text{”}\ (\text{oxide});\ \Delta G_1 < 0 \qquad [1]$$

where ΔG_1 is the Gibbs energy change for the reaction. In Reaction [1], cation **B** is displaced by cation **A** in the oxide, without changing the crystal structure of the oxide, and cation **C** does not participate in the chemical exchange reaction. During the reaction, "**B**" is typically precipitated as **A-B** alloy and the product oxide, "$\mathbf{ACO}_{m+n}$", is usually $(\mathbf{A},\mathbf{B})\mathbf{CO}_{m+n}$. The reaction is associated with a volume increase in the product zone, mainly due to the volume of "**B**" precipitate. The oxide systems in which Reaction [1] is possible are illustrated in Figure 1 and discussed in the following.

Consider three binary oxides, $\mathbf{AO}_m$, $\mathbf{BO}_m$, and $\mathbf{CO}_n$; $\mathbf{AO}_m$ and $\mathbf{BO}_m$ have the same crystal structure (different from that of $\mathbf{CO}_n$) and form a continuous series of solid solutions. Also, the thermodynamic stability of the binary oxides is such that $\Delta G^\circ(\mathbf{CO}_n) << \Delta G^\circ(\mathbf{AO}_m) < \Delta G^\circ(\mathbf{BO}_m)$. The binary oxides combine to form ternary line compounds of narrow homogeneity range, *e.g.*, $\mathbf{ACO}_{m+n}$ and $\mathbf{BCO}_{m+n}$, and having the same crystal structure. The meaning of line compound is that the ratio **A**:**C** or **B**:**C** has a constant value (equal to 1:1)* and any deviation from it will result in the

S.N.S. REDDY, Senior Engineer and L.B. WIGGINS, Senior Technical Staff Member, are with the Systems and Technology Group, IBM Corporation, Hopewell Junction, NY 12533. Contact e-mail: snreddy@us.ibm.com D.N. LEONARD, Graduate Student, is with the Department of Materials Science, North Carolina State University, Raleigh, NC 27695. K.T. JACOB, Professor, is with the Department of Metallurgy, Indian Institute of Science, Bangalore-5600 12, India.

Manuscript submitted July 13, 2004.

*Other ternary line compounds, such as $(\mathbf{A}\text{ or }\mathbf{B})_2\mathbf{CO}_{2m+n}$ or $(\mathbf{A}\text{ or }\mathbf{B})\mathbf{C}_2\mathbf{O}_{m+2n}$, referred to as (2:1) or (1:2), respectively, are not considered for the sake of simplicity. However, reactions in these compounds follow the same technical arguments that are applied to (1:1) compounds.

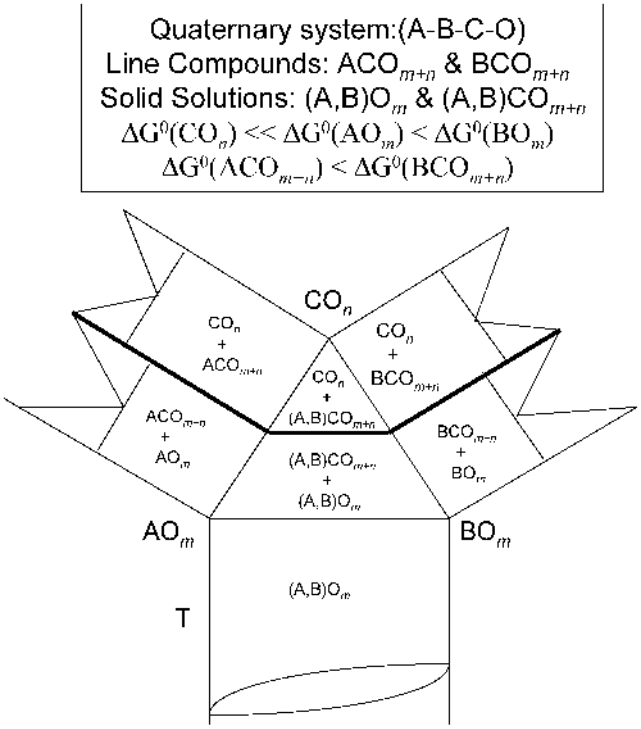

Fig. 1—Oxide system for internal displacement reaction between a metal and an oxide line compound.

decomposition of the ternary into individual binary oxides. The $\mathbf{ACO}_{m+n}$ is thermodynamically more stable than the $\mathbf{BCO}_{m+n}$, *i.e.*, ΔG° ($\mathbf{ACO}_{m+n}$) < ΔG° ($\mathbf{BCO}_{m+n}$). For convenience, it is assumed that there is no solid solubility in the end members for the systems: $\mathbf{AO}_m$-$\mathbf{CO}_n$ and $\mathbf{BO}_m$-$\mathbf{CO}_n$. The various chemical equilibria and the associated Gibbs energies for the binary and ternary oxides are

$$\mathbf{A} + (m/2)\mathbf{O}_2 = \mathbf{AO}_m;\ \Delta G^{\circ}(\mathbf{AO}_m) \quad [1]$$

$$\mathbf{B} + (m/2)\mathbf{O}_2 = \mathbf{BO}_m;\ \Delta G^{\circ}(\mathbf{BO}_m) \quad [2]$$

$$\mathbf{C} + (n/2)\mathbf{O}_2 = \mathbf{CO}_n;\ \Delta G^{\circ}(\mathbf{CO}_n) \quad [3]$$

$$\mathbf{A} + \mathbf{C} + \{(m+n)/2\}\mathbf{O}_2 = \mathbf{ACO}_{m+n};\ \Delta G^{\circ}(\mathbf{ACO}_{m+n}) \quad [4]$$

$$\mathbf{B} + \mathbf{C} + \{(m+n)/2\}\mathbf{O}_2 = \mathbf{BCO}_{m+n};\ \Delta G^{\circ}(\mathbf{BCO}_{m+n}) \quad [5]$$

$$\mathbf{AO}_m + \mathbf{CO}_n = \mathbf{ACO}_{m+n};\ \Delta G_6 = \Delta G^{\circ}(\mathbf{ACO}_{m+n}) - \Delta G^{\circ}(\mathbf{AO}_m) - \Delta G^{\circ}(\mathbf{CO}_n) \quad [6]$$

$$\mathbf{BO}_m + \mathbf{CO}_n = \mathbf{BCO}_{m+n};\ \Delta G_7 = \Delta G^{\circ}(\mathbf{BCO}_{m+n}) - \Delta G^{\circ}(\mathbf{BO}_m) - \Delta G^{\circ}(\mathbf{CO}_n) \quad [7]$$

Usually, $\Delta G_6 \approx \Delta G_7$. In addition, the decompositions of ternary compounds are defined by the following equilibria:

$$\mathbf{A} + (m/2)\mathbf{O}_2 + \mathbf{CO}_n = \mathbf{ACO}_{m+n};\ \mu_{O2} = (2/m)\{\Delta G^{\circ}(\mathbf{ACO}_{m+n}) - \Delta G^{\circ}(\mathbf{CO}_n)\} \quad [8]$$

$$\mathbf{B} + (m/2)\mathbf{O}_2 + \mathbf{CO}_n = \mathbf{BCO}_{m+n};\ \mu_{O2} = (2/m)\{\Delta G^{\circ}(\mathbf{BCO}_{m+n}) - \Delta G^{\circ}(\mathbf{CO}_n)\} \quad [9]$$

where the standard state for μ_{O2} is pure $\mathbf{O}_2$ at 1 atm pressure and the standard states for the solids are pure elements or compounds.

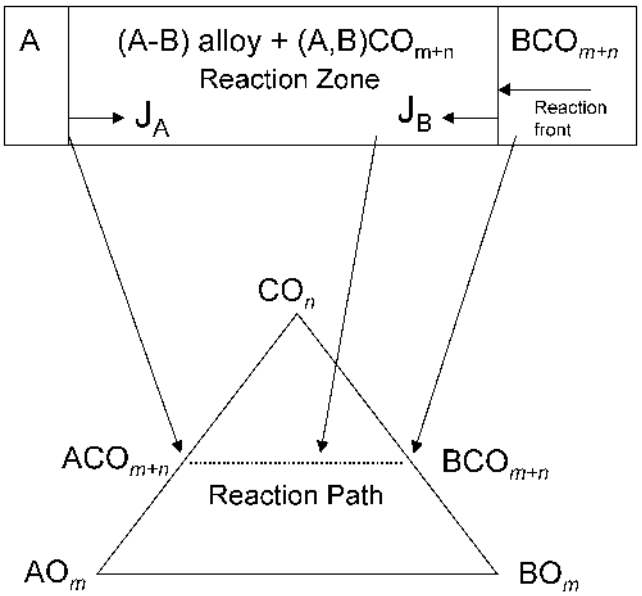

Fig. 2—Internal displacement reaction: A + BCO_{m+n} = "B" + "ACO_{m+n}".

The two ternary oxides can form solid solutions with a wide homogeneity range, $(\mathbf{A}_x\mathbf{B}_{1-x})\mathbf{CO}_{m+n}$, in which the ratio (**A** + **B**):**C** is again 1:1. In $(\mathbf{A}_x\mathbf{B}_{1-x})\mathbf{CO}_{m+n}$, cations **A** and **B** occupy a sublattice different from the sublattice for **C**. Assuming that no mixing of (**A**,**B**) and **C** is allowed, the diffusional transport of (**A**,**B**) and **C** occur in two separate sublattices and are not strongly correlated.

After the initial start of Reaction [1], the reactants are spatially separated from each other by the product phases (Figure 2):

A	//	(**A**-**B**) + $(\mathbf{A}_x\mathbf{B}_{1-x})\mathbf{CO}_{m+n}$	//	$\mathbf{BCO}_{m+n}$
A/boundary boundary I				reaction front boundary II

The overall Reaction [1] can be represented by the boundary reactions involving cation defects (vacancies or interstitials) and electrons (or electron holes). The following discussion considers the general features of cation diffusional transport and composition profile of product oxide during Reaction [1]. The discussion is qualitative and phenomenological; no emphasis is given for the point defect structure responsible for cation transport. Also, it is assumed that $D_{\mathbf{O}} << D_{\text{cation}}$ and t_e (or t_h) ≈ 1.

III. BOUNDARY CHEMICAL POTENTIALS AND CATION TRANSPORT DURING REACTION [1]

Reaction [1] is illustrated schematically in Figure 2. During the reaction, chemical potential gradients develop for all components in the product zone. Because the reacting system has four components and only a maximum of two phases coexist at a given location in the reaction zone, the chemical potentials are not uniquely defined in the reaction zone. However, relative magnitudes at the **A**/reaction zone boundary (boundary I) and the reaction front (boundary II) can be specified.

After the start of the initial reaction, when $\Delta G_1 << 0$, the composition of oxide at boundary I is essentially $\mathbf{ACO}_{m+n}$

in equilibrium with pure **A**. Similarly, at boundary II, the precipitate is essentially pure **B** in equilibrium with $\mathbf{BCO}_{m+n}$.

The chemical potentials of the other components at the boundaries are not independent and uniquely defined. Instead, they are related through various chemical equilibria, (Eqs. [2] through [10]). For example, the μ_{O2} values are not uniquely defined at boundaries I and II. However, μ^{I}_{O2} and μ^{II}_{O2} values are bounded by the oxidation of metal (**A** or **B**) as an upper limit (Eqs. [1] and [2]) and the decomposition of the ternary oxide ($\mathbf{ACO}_{m+n}$ or $\mathbf{BCO}_{m+n}$) as a lower limit (Eqs. [8] and [9]), as in

$$(2/m)\Delta G^{o}(\mathbf{AO}_m) \geq \mu^{I}_{O2} \geq (2/m)\{\Delta G^{o}(\mathbf{ACO}_{m+n}) - \Delta G^{o}(CO_n)\} \quad [10]$$

$$(2/m)\Delta G^{o}(\mathbf{BO}_m) \geq \mu^{II}_{O2} \geq (2/m)\{\Delta G^{o}(\mathbf{BCO}_{m+n}) - \Delta G^{o}(CO_n)\} \quad [11]$$

Given that ΔG^{o} ($\mathbf{ACO}_{m+n}$) $< \Delta G^{o}$ ($\mathbf{BCO}_{m+n}$) and ΔG^{o} ($\mathbf{AO}_m$) $< \Delta G^{o}$ ($\mathbf{BO}_m$), it is clear that $\mu^{I}_{O2} < \mu^{II}_{O2}$. To summarize, during Reaction [1]:

Boundary I	Boundary II
low μ_{O2}	high μ_{O2}
high μACO_{m+n}	low μACO_{m+n}
low μBCO_{m+n}	high μBCO_{m+n}
high μ_A	low μ_A
low μ_B	high μ_B

The general flux equations for cation diffusion during Reaction [1] are

$$J_{\mathbf{A}}(\rightarrow) = -L_{\mathbf{AA}}\nabla\mu_{\mathbf{A}} - L_{\mathbf{AB}}\nabla\mu_{\mathbf{B}} \quad [12]$$

$$J_{\mathbf{B}}(\leftarrow) = -L_{\mathbf{AB}}\nabla\mu_{\mathbf{A}} - L_{\mathbf{BB}}\nabla\mu_{\mathbf{B}} \quad [13]$$

The arrows represent the flux direction as ($\rightarrow$) toward boundary II or the reaction front, and ($\leftarrow$) toward sboundary I or the **A**/product zone boundary. Because both **A** and **B** occupy the same sublattice and diffuse by the same point-defect mechanism, the cross-coefficients can be significant. In Eqs. [13] and [14], when the transport cross-coefficient $L_{\mathbf{AB}} > 0$, the fluxes due to $L_{\mathbf{AB}}$ terms are opposite to the fluxes due to terms containing $L_{\mathbf{AA}}$ or $L_{\mathbf{BB}}$. In this case, the effect of the cross-coefficient is to decrease the magnitude of $J_{\mathbf{A}}$ and $J_{\mathbf{B}}$. The composition profile of the product oxide in the reaction zone is illustrated schematically in Figure 3.

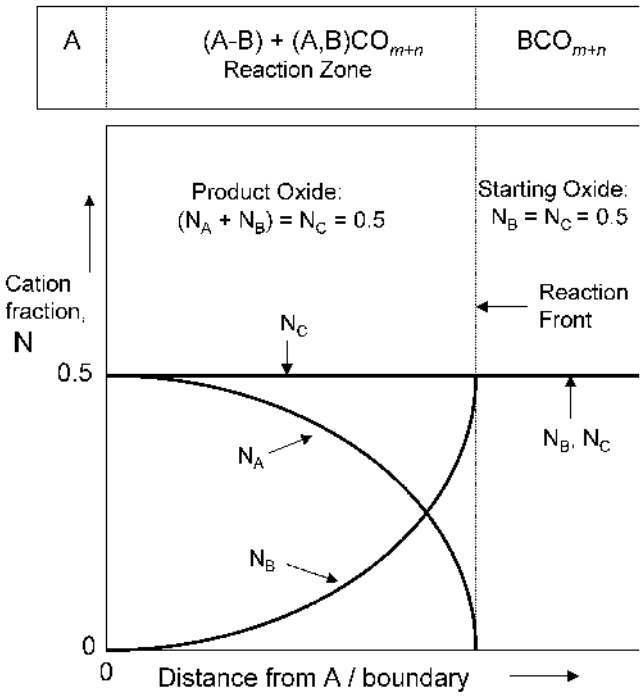

Fig. 3—Composition profile of oxide for the reaction: A + BCO_{m+n} = "B" + "ACO_{m+n}".

IV. REACTION BETWEEN Fe AND $NiTiO_3$ AT 1273 K

As an example of Reaction [1], the following reaction was studied at 1273 K as a function of time:

$$Fe + NiTiO_3 = \text{"Ni"} + \text{"}FeTiO_3\text{"} \quad [14]$$

where "$FeTiO_3$" is present in the mixed oxide, $(Fe,Ni)TiO_3$, formed by the displacement of Ni by Fe in the starting oxide, and "Ni" is precipitated as a γ-(Fe-Ni) alloy. The reaction was studied using both single-crystal and polycrystalline $NiTiO_3$.

The ilmenite structure of $FeTiO_3$ and $NiTiO_3$ is hexagonal close-packed, which is an ordered derivative of Corundum. The two cationic sublattices are alternating sheets of Fe^{2+}/Ni^{2+} and Ti^{4+} with octahedral coordination. There is evidence[13] to show that Fe^{3+} and Ti^{3+} are not compatible in ilmenite. Although no experimental data are available, it is expected that $NiTiO_3$ and $FeTiO_3$ are soluble in each other, resulting in the formation $(Fe,Ni)TiO_3$ solid solution. From the available data for $NiTiO_3$[14] and $FeTiO_3$,[14,15] the standard Gibbs energy change for Reaction [14], at 1273 K, is estimated to be -66.1 kJ/mol.

During Reaction [2], it is expected that Fe diffuses toward the reaction front with a counter-diffusion of Ni toward the Fe/boundary. As such, concentration gradients will develop for both Fe and Ni in the product oxide. If there is no decomposition of the ilmenite structure during the reaction, the Ti fraction in the product oxide should remain constant across the reaction zone.

V. EXPERIMENTAL PROCEDURE

Sintered polycrystalline $NiTiO_3$ discs were prepared starting from the powdered compound (99.9 pct pure, Cerac, Inc, Milwaukee, WI). The powder was pressed into 12-mm discs using an organic binder and sintered in air, at 1073 K for 1 hour and at 1673 K for 45 hours; the discs were then annealed for 240 hours at 1273 K in air. The faces of the discs were ground with successively finer SiC paper and polished with 3-μm diamond paste. An X-ray diffraction analysis of the starting powder and sintered disc confirmed the ilmenite structure of $NiTiO_3$, and any other phases were below the detection limit. Also, a scanning electron microscope (SEM) examination of the sintered discs did not show the presence of any minor phases such as NiO and TiO_2.

Single-crystal $NiTiO_3$ was prepared by heating rutile (TiO_2) single-crystal discs (2-mm thick, random orientation) inside a Pt crucible and packed with excess NiO powder

(99 pct pure, Cerac Inc.) on all sides. The conversion of TiO_2 into $NiTiO_3$ was done at 1673 K in air for a period of 500 hours. On cooling, a cross-sectional examination showed that a thick layer of $NiTiO_3$ ($\sim$1 mm) was formed on all surfaces with a thin central core of unreacted TiO_2. The ilmenite structure of the thick outer layer was confirmed by X-ray diffraction. The titanate was essentially single crystal, with cracks developing along the reaction direction, probably formed during cooling due to the thermal expansion difference between the TiO_2 core and the thick titanate on the surface. The $NiTiO_3$ between cracks can be considered as single-crystal grains having the same (unknown) orientation. The diameter of each titanate grain between cracks was larger than the thickness of product zone for Reaction [14]. The surfaces of single-crystal titanate discs were polished with 3-μm diamond paste before use.

The Fe discs were cut from foil with a purity of 99.995 pct (Puratronic grade, Johnson Matthey, Ward Hill, MA). The surfaces were polished with 3-μm diamond paste and washed in deionized (DI) water before use.

To start the experiment, $NiTiO_3$/Fe discs were sandwiched between two flat alumina plates with a load of about 5 kg/cm^2 and placed inside an INCONEL* muffle of the resistance furnace. The atmosphere during the reaction was flowing high-purity N_2 with less than 1 ppm of oxygen or moisture. The reaction couple was also surrounded by a "tent" of Cu foils. The samples were heated at a rate of 20 K/min to 1273 K, held constant within $\pm$2 K for a specified time, and cooled to room temperature by turning off the power to the furnace. The reacted couple were sectioned, mounted, polished, and examined under an optical microscope, and photographed at known magnification. Some specimens were examined in an SEM and the compositions in the reaction zone were analyzed using electron-probe microanalysis (EPMA).

*INCONEL is a trademark of INCO Alloys International, Huntington Woods, WV.

VI. RESULTS

A. *Reaction with Polycrystalline $NiTiO_3$*

The reaction between Fe and sintered polycrystalline $NiTiO_3$ at 1273 K for 64 hours is shown in Figure 4; Figure 4(a) is a cross-sectional view along the reaction direction and Figure 4(b) is a transverse view perpendicular to the reaction direction close to the Fe interface, obtained after removing the Fe layer. The original Fe/$NiTiO_3$ interface is about 140 μm inside the reaction zone. There is less porosity in the reaction zone than in the starting oxide. The volume increase in the product zone accompanying the displacement reaction is approximately 25 pct. An X-ray diffraction analysis of the reaction zone showed only the lines corresponding to the ilmenite structure and the γ phase of Ni-Fe system. The majority of the Ni-Fe alloy is interconnected and seems to be precipitated along the grain boundary, with some smaller precipitates inside the grains.

The composition of both the oxide and the Ni-Fe alloy phases in the reaction zone were analyzed by EPMA as a function of distance from the Fe/boundary, and are shown in Figure 5 for a reaction time of 64 hours. Care was taken to focus a narrow electron beam on either the oxide (gray phase in Figure 4) or the Ni-Fe alloy (bright phase), in order to minimize the interference from the neighboring phases. The concentration profiles for all the cations in the product oxide are consistent with the ilmenite structure and the displacement of Ni by Fe in the starting oxide. Near the Fe/boundary, the Ni is essentially completely replaced by the Fe and the composition is close to $FeTiO_3$; the Fe content of (Fe,Ni)TiO_3 decreases away from the Fe interface; and at the reaction front, the oxide composition is $NiTiO_3$. The Ti content of the oxide phase is constant throughout the reaction zone (the same as in the original oxide), as is expected when the ilmenite structure, (Fe,Ni)TiO_3, is maintained during the reaction with very little decomposition into component oxides. The starting $NiTiO_3$ composition is maintained beyond the reaction front. The alloy precipitate is approximately $Ni_{0.7}Fe_{0.3}$ near the Fe/reaction zone boundary and becomes progressively richer in Ni toward the reaction front, approaching 100 pct Ni at the reaction front.

Figure 6 is an SEM image showing the presence of a minor phase consisting of small TiO_2 islands ($<$5 pct) in the middle of the reaction zone, which is predominantly (Fe,Ni)TiO_3 + γ alloy. The X-ray imaging of the region, shown in Figure 7, confirms that the dark gray phase in Figure 6 are rutile particles embedded in ilmenite matrix (light gray). The presence of TiO_2 in the product zone is unexpected and suggests that it was either present in the starting $NiTiO_3$ powder or was formed during the displacement reaction, possibly by ilmenite decomposition. The X-ray diffraction of the starting $NiTiO_3$ powder did not show any significant presence of TiO_2. The possibility of the kinetic decomposition of the ilmenite structure as a source of TiO_2 is given in Section VII.

A. *Reaction with Single-Crystal $NiTiO_3$*

The reaction between the Fe and the single-crystal $NiTiO_3$ at 1273 K and 25 hours is shown in Figure 8 as a cross-sectional view along the direction of the reaction. The bright phase is Ni-Fe alloy and the gray phase is ilmenite. Figure 8(a) represents the entire reaction zone; Figure 8(b) is near the Fe/boundary; and Figure 8(c) is near the reaction front. A vertical feature of the alloy in Figure 8(a) is due to the presence of a crack in the starting oxide. The γ-alloy precipitate has an elongated ribbonlike structure and seems to be arranged in layers, in contrast to the sintered $NiTiO_3$, in which grain boundary precipitation was predominant. The alloy layers are not continuous; the crystallographic orientation relationship between alloy and ilmenite phases, if it exists, is not clear. The distribution of the γ alloy close to the Fe/boundary, along a plane approximately normal to the reaction direction, is shown in Figure 9. It is clear from Figures 8 and 9 that pores (dark regions) develop at the edges of the alloy precipitate, due to the condensation of vacancies during precipitation. The reaction zone was examined in an SEM under high magnification for the presence of any rutile or wustite phases formed during Reaction [14]. The reaction zone consists of γ alloy and ilmenite phases only, without any trace of rutile or wustite phase.

The composition of the product oxide phase for the reaction between the Fe and the single-crystal $NiTiO_3$, as determined by EPMA, is shown in Figure 10. The composition data are very similar to those using sintered $NiTiO_3$

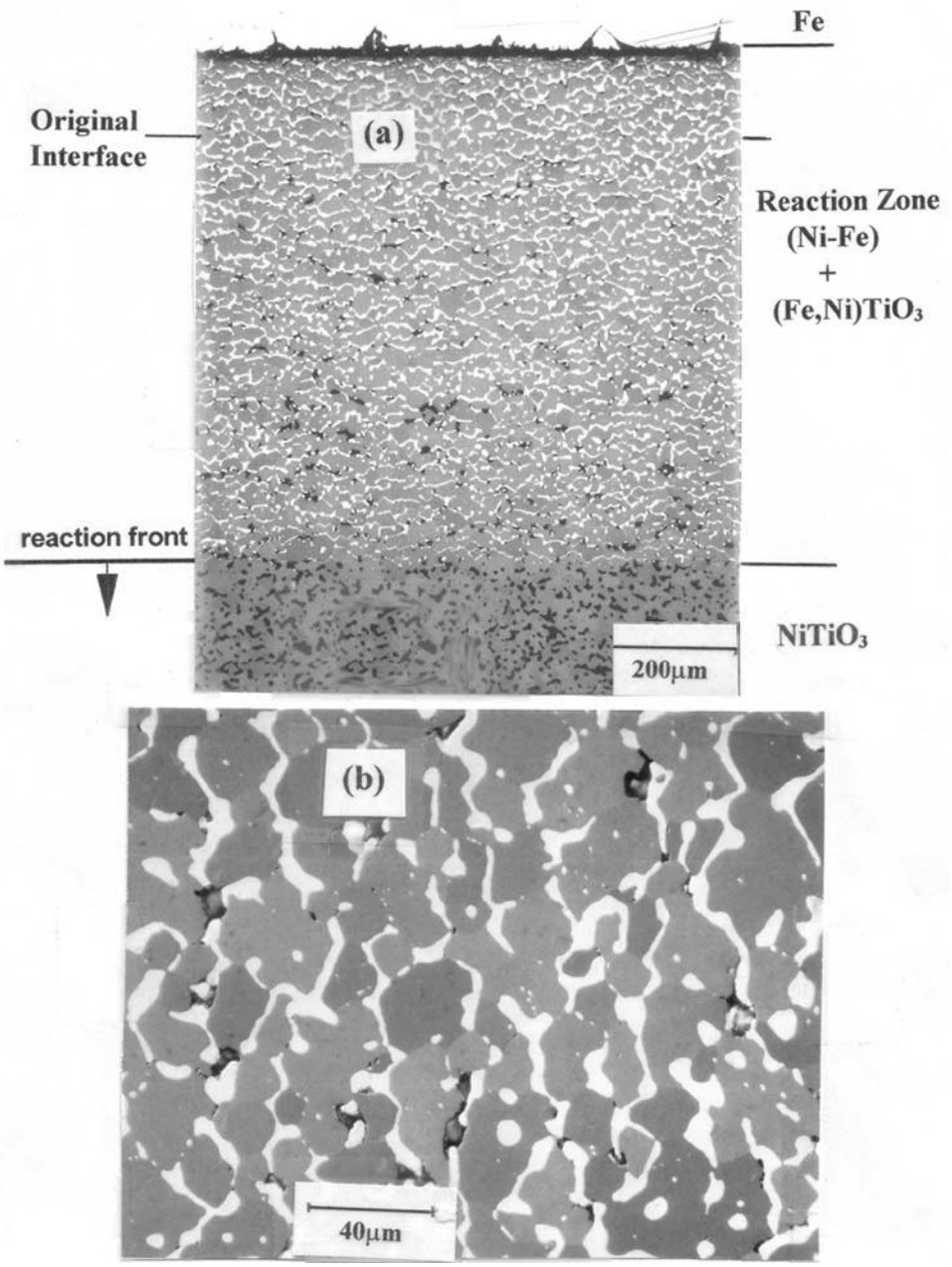

Fig. 4—Reaction zone between Fe and polycrystalline $NiTiO_3$ at 1273 K and 64 h: (*a*) cross-sectional view and (*b*) transverse section, perpendicular to the reaction direction, near the Fe interface. Bright phase: γ alloy; and gray phase: $(Fe,Ni)TiO_3$.

in Figure 5 and are consistent with ilmenite composition within 6 pct. In Figure 10, the minor deviation of (Ni + Fe):Ti from a 1:1 ratio (*i.e.*, higher Ti and lower Ni + Fe) is attributed to measurement error during EPMA, possibly related to machine calibration; this is also reflected in the analysis of unreacted $NiTiO_3$. If the starting $NiTiO_3$ crystal were to be considered as the source of calibration, the deviation from the exact cation ratio required for the ilmenite structure disappears.

In reaction with the single-crystal $NiTiO_3$, an EPMA analysis of γ-alloy precipitate, without interference from the neighboring oxide phase, was difficult because of the narrow width of the precipitate. However, measurements at selected locations indicated that the composition profile was very similar to that in reactions using sintered polycrystalline $NiTiO_3$.

The kinetics of the $Fe/NiTiO_3$ reaction follows parabolic behavior, as shown in Figure 11, where the reaction zone thickness is plotted against the square root of time. The data for both polycrystalline and single-crystal $NiTiO_3$ are similar, indicating that the influence of grain boundary diffusion and precipitation on reaction kinetics is not significant. From the combined data, the rate constant, defined as $(\text{thickness})^2/2 \times (\text{time})$, is given by

$$k_p = 1.3 \times 10^{-12}\ m^2 s^{-1} \qquad [15]$$

VII. DISCUSSION

The composition profiles of the product oxide (Figures 5 and 10) in the reaction zone are consistent with the selective

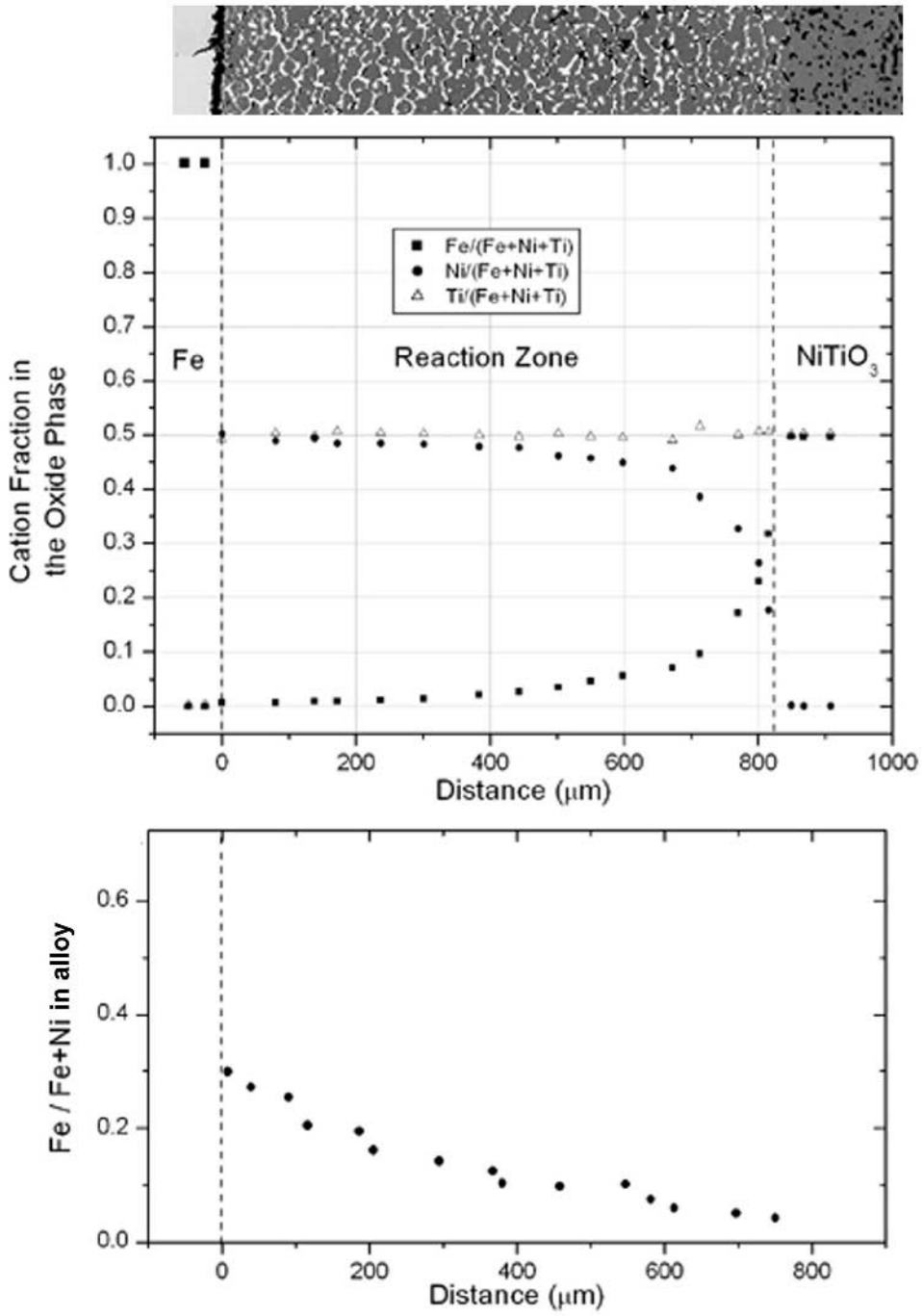

Fig. 5—Composition of the oxide and alloy phases in the product zone for the reaction between Fe and polycrystalline $NiTiO_3$. The $T = 1273$ K and $t = 64$ h.

displacement of Ni cations in $NiTiO_3$ with Fe, without changing the crystal structure of ilmenite. During the reaction, Fe diffuses toward the reaction front, accompanied by a counter flux of Ni toward the Fe/boundary. The fluxes are given by Eqs. [12] and [13], where **A** and **B** are Fe and Ni, respectively. As such, concentration gradients develop in the Ni/Fe sublattice of the product oxide. There is no net flux in the Ti sublattice, and its concentration remains constant across the reaction zone. It is possible, in principle, to model the composition profile of the product ilmenite in the reaction zone, provided that D_{Fe} and D_{Ni} in $(Fe,Ni)TiO_3$ are known as a function of composition and oxygen partial pressure. However, there are no experimental data on cation disorder and diffusion in $(Fe,Ni)TiO_3$ at 1273 K as a function of composition and oxygen partial pressure.

The possible point defects in the cation sublattice of $(Fe,Ni)TiO_3$ are either due to thermal disorder or to nonstoichiometry. Neglecting any nonstoichiometry in ilmenite, the possible cation defects due to thermal disorder are as follows: (1) Schottky disorder with vacancies in both sublattices V_{Ni} and V_{Ti}, (2) interstitials only in both sublattices Ni_I and Ti_I, and (3) Frenkel disorder of vacancies and interstitials: V_{Ni}, Ni_I, or V_{Ti}, Ti_I.

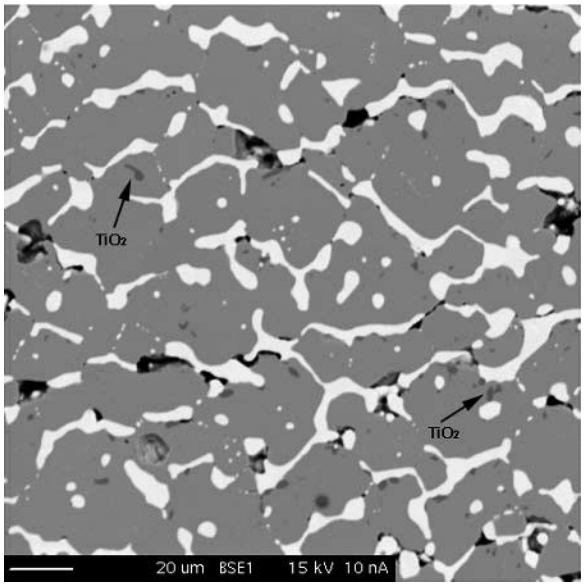

Fig. 6—An SEM image showing the presence of TiO_2 particles in the middle of the reaction zone between Fe and polycrystalline $NiTiO_3$. Bright phase: γ alloy; light gray: (Fe,Ni)TiO; and dark gray: TiO_2.

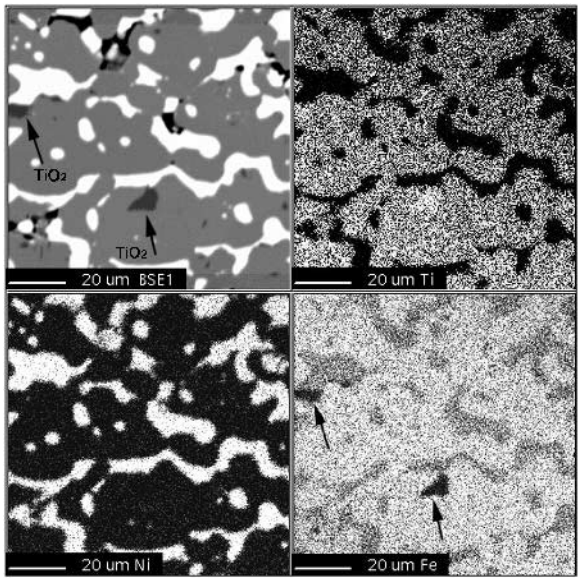

Fig. 7—The X-ray dot maps of Ti, Ni, and Fe in the reaction zone containing TiO_2 particles.

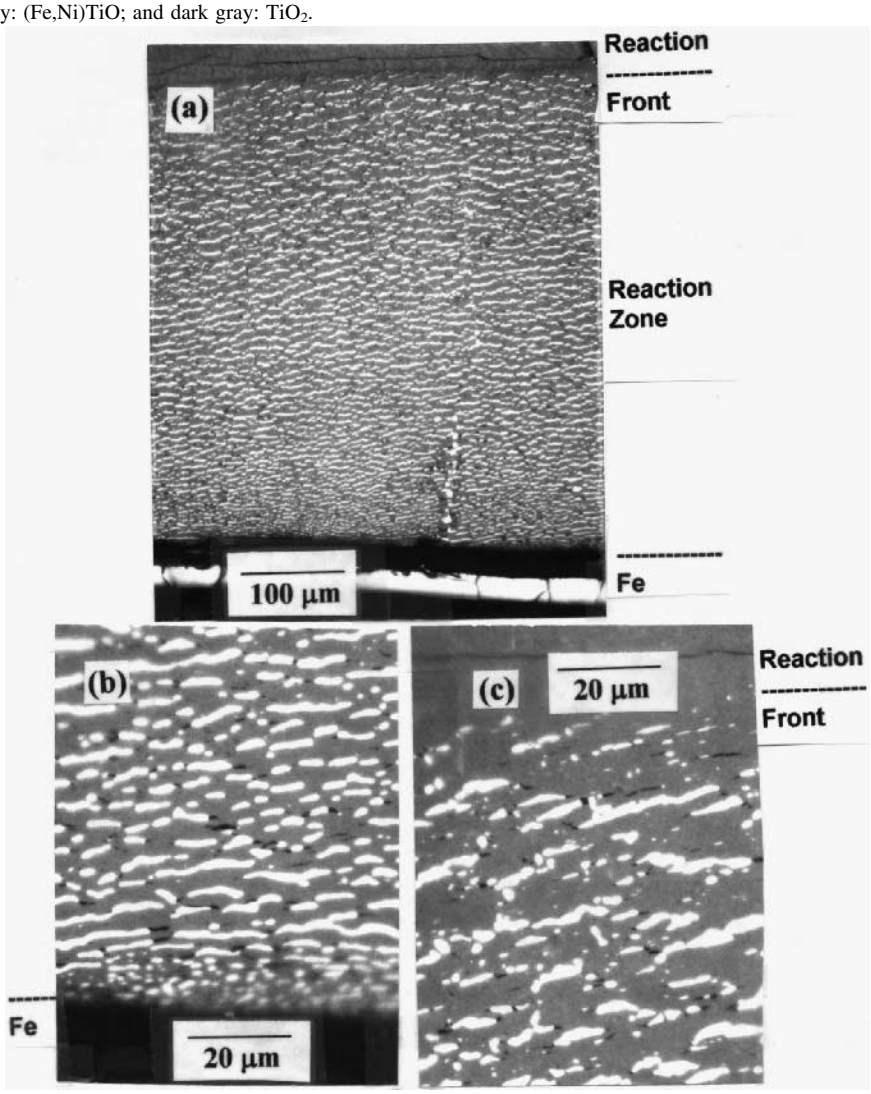

Fig. 8—Reaction between Fe and single-crystal $NiTiO_2$ at 1273 K and 25 h: (*a*) complete reaction zone, (*b*) region near the Fe/boundary, and (*c*) region near the reaction front. The bright phase is γ-(Ni,Fe) alloy; the gray phase is $(Fe,Ni)TiO_3$; and the dark spots are porosity.

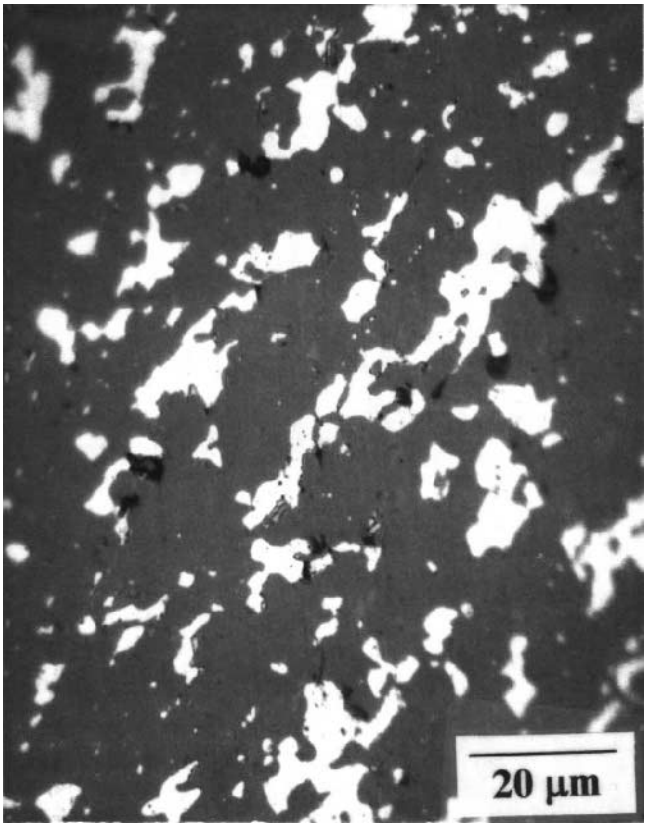

Fig. 9—The Fe/single-crystal $NiTiO_3$ reaction at 1273 K and 25 h. Transverse view (*i.e.*, normal to the reaction direction) of the reaction zone near the Fe/boundary.

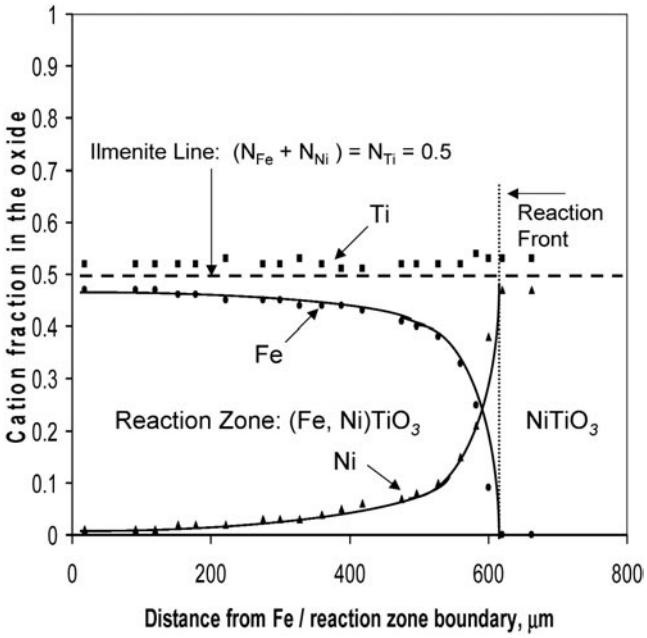

Fig. 10—The EPMA analysis of the oxide composition in the product zone for the reaction between Fe and single-crystal $NiTiO_3$ at 1273 K; t = 49 h. (Note: The EPMA points correspond to the ilmenite composition within 6 pct; the lines are drawn for visual recognition purpose only).

Not all possible defects are equally significant; on energetic grounds, one type of disorder is more favored and it dominates the cation diffusion process. In addition to thermally created defects, any nonstoichiometry can introduce one type of point defect (vacancy or interstitial), with a concentration much higher than that of the other defects; at a constant temperature, T, the defects due to nonstoichiometry are strong functions of the composition (Ni/Fe ratio) and the oxygen partial pressure. For the discussion of displacement Reaction [14] only the point defects in the Ni/Fe sublattice are important for cation diffusion. Since no data are available, it is not possible to write the displacement reaction mechanism in terms of the majority point defects. However, assuming that Fe/Ni diffusion occurs mainly through a vacancy mechanism, the boundary reactions can be written as the following.

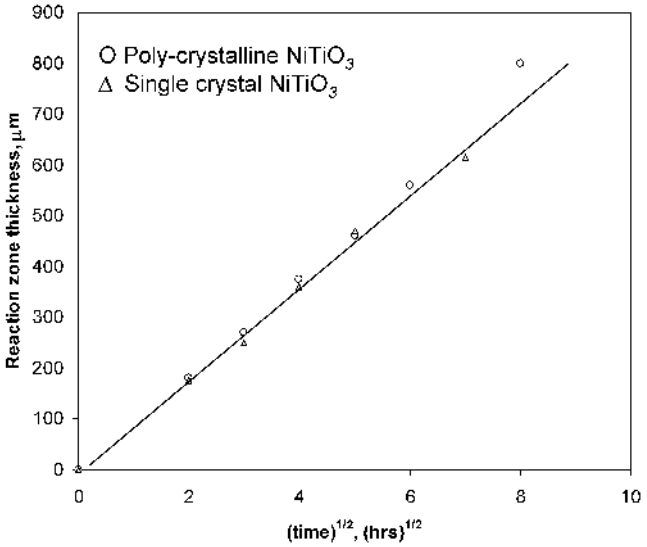

Fig. 11—The kinetics of the displacement reaction between Fe and $NiTiO_3$.

(a) The Fe/product oxide zone boundary (Fe dissolution and vacancy annihilation): Fe (metal) + V_{Ni} (ilmenite) = Fe^{2+} (ilmenite) + $2e^-$ (ilmenite).
(b) The reaction front (Ni precipitation and vacancy generation): Ni^{2+} (ilmenite) $+2\,e^-$ (ilmenite) = Ni (γ alloy) + V_{Ni} (ilmenite).

Similar boundary reactions can be written if interstitials are responsible for Fe/Ni diffusion.

As shown in Figure 11, the reaction rates are similar for either polycrystalline or single-crystal $NiTiO_3$ as the starting oxide. This indicates that the kinetics is controlled by the lattice diffusion of Fe and Ni, and that any contribution of diffusion along grain boundaries is negligible. The grain boundaries in polycrystalline oxide act as preferred nucleation sites for γ-alloy precipitates, as is evident in Figure 4. Since the diffusion data for Ni and Fe are not available, it is not possible to relate the magnitude of the rate constant to the transport properties in $(Ni,Fe)TiO_3$.

In the case of single-crystal $NiTiO_3$ as the starting oxide, the γ-alloy precipitates are elongated ribbons in layered arrangement perpendicular to the diffusion direction. An interesting question is whether the precipitation process follows the Liesegang-type phenomenon, which is related to cation diffusion combined with buildup of supersaturation before the nucleation of γ phase. (In polycrystalline $NiTiO_3$, the grain boundaries provide easy heterogeneous nucleation

sites and a layered structure is not observed). A well-known characteristic of Liesegang precipitation is the relationship between the layer separation and the layer sequence as the distance increases from the Fe/boundary, as in

$$(\Delta x_n/x_n) = (x_{n+1} - x_n)/x_n = K \text{ (constant)} \qquad [16]$$

where x_n is the distance of nth precipitate layer from the Fe/boundary. This phenomenon is more common in dilute precipitating systems (*e.g.*, References 16 and 17); the applicability of Eq. [16] for concentrated systems such as Reaction [14] is not clear. An attempt was made to check Eq. [16] for the layered γ-alloy precipitate in single-crystal $NiTiO_3$ (Figure 8). Because of the discontinuous layers in the γ phase, in a single two-dimensional micrograph, not all the precipitate layers are present along a line in the diffusion direction. Using micrographs at different depths of the reaction zone and measuring along different lines in the diffusion direction, the data shows that Δx_n increases systematically with x_n and are suggestive of Eq. [16]. However, because the precipitating system is concentrated and the data show large scatter, the constant K in Eq. [16] could not be determined accurately.

Finally, a brief discussion is necessary to account for the small numbers of TiO_2 particles observed in the product zone, when the starting oxide is polycrystalline $NiTiO_3$. It cannot be ruled out that a minor "kinetic decomposition" of the ilmenite structure occurs during the cation diffusion processes responsible for Reaction [14]. The kinetic decomposition of ilmenite is not possible when the counterfluxes J_{Fe} and J_{Ni} are equal in magnitude and $J_{Ti} = 0$ during the displacement reaction. However, because of the oxygen chemical potential gradient across the reaction zone, a small flux of both Ti and Fe/Ni is directed toward the reaction front (these minor fluxes are in addition to the major counter fluxes of Fe and Ni due to the displacement reaction). The decomposition occurs when the minor fluxes are such that $J_{Ti} \neq \Sigma J_{Fe,Ni}$ or the ratio $\beta = D_{Fe(Ni)}/D_{Ti}$ is substantially different from 1. The kinetic decomposition of initially homogeneous $NiTiO_3$ subjected to oxygen chemical potential gradients has been observed and discussed by Schmalzreid and Laqua.[18,19] The decomposition products are as follows: (1) a rutile phase (without any NiO in solution) at the side of low oxygen pressure, and (2) a (Ni,Ti)O wustite phase (*i.e.*, NiO containing dissolved TiO_2) at the side of high oxygen pressure, indicating $\beta > 1$. Following similar arguments, when pure initially homogeneous $FeTiO_3$ is maintained under a sufficient oxygen partial pressure gradient at 1273 K, the expected decomposition products, based on the phase diagram[20] and $D_{Fe} > D_{Ti}$, are TiO_2 at a low oxygen partial pressure boundary and Fe_2TiO_4 at a high oxygen partial pressure boundary. Given the composition of the ilmenite phase during Reaction [14], the expected phases due to kinetic decomposition are TiO_2 at the Fe/boundary and (Ni,Ti)O at reaction front. Also, from the phase diagram,[20] the solubility of wustite is negligible in rutile near the Fe/boundary, and the reaction rate should decrease drastically after some initial time because of the reduced Fe transport. Such behavior was not observed in the current experiments. Instead, very minor amounts of TiO_2 were distributed, more or less uniformly, in the reaction zone, and the rate constant was unchanged for up to 64 hours. Thus, it is unlikely that the product oxide layer undergoes kinetic decomposition after its formation. Another possible explanation for the presence of TiO_2 is the kinetic decomposition of unreacted $NiTiO_3$ exposed to an oxygen potential gradient throughout the experiment: one side of the disc is in contact with the Ni-Fe alloy ($\sim$100 pct Ni) at the reaction front and the other side is exposed to nitrogen gas, which might have an higher oxygen partial pressure because of trace oxygen molecules present. The unreacted disc can kinetically decompose during the experiment, producing TiO_2 particles near the reaction front. As the displacement reaction proceeds, these TiO_2 particles, formed by the kinetic decomposition of unreacted $NiTiO_3$, get incorporated into the product layer. In this case, there should be excess "NiO" phase present on the side of the disc exposed to nitrogen gas; this was not detected. Consequently, the source of the rutile phase in the product oxide ($<$5 vol pct) is not clear. Based on these observations, it is highly unlikely that any kinetic decomposition of ilmenite occurred during Reaction [14]. The most probable source for rutile is the starting $NiTiO_3$ powder, even though X-ray diffraction was unable to detect it; additional evidence for this is the absence of any trace amounts of TiO_2 in the product zone when the starting oxide is single-crystal $NiTiO_3$.

VIII. SUMMARY

Internal displacement reactions in an oxide compound with a narrow homogeneity range were studied using an Fe/$NiTiO_3$ reaction couple at 1273 K. The starting oxide was both single-crystal and sintered polycrystalline discs. During reaction, Fe displaces Ni in the oxide maintaining the ilmenite crystal structure and Ni is precipitated as a Ni-Fe (γ) alloy. The displacement is nearly complete near the Fe/reaction zone boundary and decreases towards the reaction front. The γ alloy tends to precipitate along grain boundaries in polycrystalline samples; in single-crystal oxide, the alloy precipitate is elongated and has a layered structure. Concentration gradients develop for both the oxide and the alloy precipitate in the product zone. The alloy has highest the Fe concentration ($\sim$30 at. pct) near the Fe/product zone boundary, and becomes progressively richer in Ni toward the reaction front. The product oxide exhibits a concentration gradient for Fe and Ni, but not for Ti, consistent with the ilmenite structure. The parabolic rate constant for the reaction at 1273 K is $k_p = 1.3 \times 10^{-12}$ m^2 s^{-1}. In the case of single-crystal $NiTiO_3$ as the starting oxide, the γ-alloy precipitate is probability a Liesegang-type phenomenon, which is indicative of the supersaturation required for γ-alloy precipitate nucleation.

REFERENCES

1. R.A. Rapp, A. Ezis, and G.J. Yurek: *Metall. Trans.*, 1973, vol. 4, p. 1283.
2. G.J. Yurek, R.A. Rapp, and J.P. Hirth: *Metall. Trans.*, 1973, vol. 4, p. 1293.
3. S.N.S. Reddy and L.B. Wiggins: *Metall. Mater. Trans. A*, 2002, vol. 33A, p. 2899.
4. C. Tangchitvittaya, J.P. Hirth, and R.A. Rapp: *Metall. Trans. A*, 1982, vol. 13A, p. 585.
5. D.W. Song, R. Subramanian, and R. Dieckmann: *Mater. Res. Symp. Proc.*, 1995, vol. 365, p. 59.
6. J.P. Smith, P. Limthongkul, and S.L. Sass: *Acta Mater.*, 1997, vol. 45, p. 4241.
7. R.A. Rapp: *Corrosion*, 1965, vol. 8, p. 889.
8. H. Schmalzried: *Ber. Bunsenges. Phys. Chem.*, 1983, vol. 87, p. 51.
9. H. Schmalzried: *Ber. Bunsenges. Phys. Chem.*, 1984, vol. 88, p. 1186.

10. H. Schmalzried and M. Backhaus-Ricoult: *Progr. Solid State Chem*., 1993, vol. 22, p. 1.
11. R.L. Shook, R.A. Rapp, and J.P. Hirth: *Metall. Trans. A*, 1985, vol. 16A, p. 1815.
12. S.N.S. Reddy, D.N. Leonard, L.B. Wiggins, and K.T. Jacob: *Metall. Mater. Trans. A*, 2005, vol. 36A, pp. 2695-2703.
13. W. Simons and E. Woermann: *Contrib. Mineral. Petrol*., 1978, vol. 66, p. 81.
14. R.W. Taylor and H. Schmalzried: *J. Phys. Chem*., 1964, vol. 68, p. 2444.
15. G.M. Kale and K.T. Jacob: *Metall. Trans. B*, 1991, vol. 23B, p. 57.
16. V.A. Van Rooijen, E.W. Van Royen, J. Vrigen, and S. Radelaar: *Acta Metall*., 1975, vol. 23, p. 987.
17. D. Ricoult and H. Schmalzried: *Ber. Bunsenges. Phys. Chem*., 1986, vol. 90, p. 135.
18. H. Schmalzried and W. Laqua: *Oxid. Met*., 1981, vol. 15, p. 339.
19. W. Laqua, and H. Schmalzried: in *High Temperature Corrosion*, R.A. Rapp, ed., NACE, Houston, TX, 1983, p. 115.
20. G. Eriksson and A.D. Pelton: *Metall. Trans. B*, 1993, vol. 24B, p. 795.